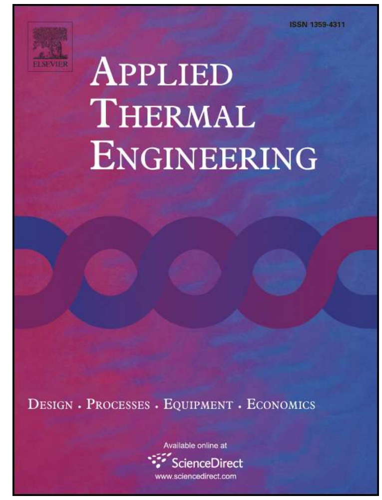

Research Paper

Inhomogeneity in pore size appreciably lowering thermal conductivity for porous thermal insulators

Lin Qiu, Hanying Zou, Dawei Tang, Dongsheng Wen, Yanhui Feng, Xinxin Zhang

PII: S1359-4311(17)34800-7
DOI: https://doi.org/10.1016/j.applthermaleng.2017.11.066
Reference: ATE 11436

To appear in: *Applied Thermal Engineering*

Received Date: 20 July 2017
Revised Date: 8 October 2017
Accepted Date: 13 November 2017

Inhomogeneity in pore size appreciably lowering thermal conductivity for porous thermal insulators

Lin Qiu[a,b], Hanying Zou[a,b], Dawei Tang[c], Dongsheng Wen[d], Yanhui Feng[a,b*], Xinxin Zhang[a,b]

[a] School of Energy and Environmental Engineering, University of Science and Technology Beijing, Beijing 100083, China

[b] Beijing Key Laboratory of Energy Saving and Emission Reduction for Metallurgical Industry, University of Science and Technology Beijing, Beijing 100083, China

[c] Key Laboratory of Ocean Energy Utilization and Energy Conservation of Ministry of Education, Dalian University of Technology, Dalian 116024, China

[d] School of Chemical and Process Engineering, University of Leeds, Leeds, LS2 9JT, UK

[*] Corresponding author. Prof. Yanhui Feng. Email: yhfeng@me.ustb.edu.cn

HIGHLIGHTS:

- Quantitative degradation effect of inhomogeneity in pore size is first revealed.
- Adaptable interfacial sensor technology is proposed to ensure accurate measurement.
- Ample models of heat transfer are compared to extract the inhomogeneity effect.
- This study opens up fresh opportunities for developing super thermal insulators.

ABSTRACT: It has been years since the concept that inhomogeneity in pore size has an adverse effect on the thermal transport came into view. Typically, although some porous materials possess the identical porosity, they could show a strong inhomogeneity in pore size, making the physical parameters change greatly. However, one major and often overlooked challenge in understanding the underlying mechanism behind the above observation involves quantifying the effect of inhomogeneity. In this paper, the inhomogeneity in pore size is quantitatively evaluated to explain the thermal conductivity diminishment in the porous material system. By means of self-developed adaptable interfacial thermo-sensor technology, the thermal conductivity of a series of micro-porous foams with homogeneous pores are accurately characterized, and its evolution trend versus porosity agrees well with the typical homogeneous model. To compare with homogeneous materials, the thermal conductivity of the inhomogeneous porous materials is calculated by coupling 3D tomographic modeling and finite element method. An appreciable thermal conductivity reduction up to 13.5% is found as a result of the constructed inhomogeneity for pore size distribution. Furthermore, the distinction between the homogeneous and inhomogeneous models would remarkably diminish as the porosity approaches a very high value, probably owing to the increment of the content of the solid-gas interface. Our work opens up fresh opportunities for research of super thermal insulation materials. In contrast to harnessing high porosity, developing inhomogeneity in pore size distribution could play a critical role in further lowering the thermal conductivity of porous thermal insulators.

KEYWORDS: Inhomogeneity in pore size distribution; Adaptable interfacial sensor; Thermal conductivity; Reconstruction modeling; 3ω technique

1. Introduction

The research in thermal transport on the basis of homogeneous porous material systems have proved that the density or porosity plays a pivotal role in the apparent thermal conductivity [1-4], and in order to produce super thermal insulators, materials with high porosity have been pursued for many decades [5-7]. However, with the roaring needs of excellent lightweight thermal insulators to fulfill our mission of space exploration [8], a further limitation of thermal transport in the porous materials is urgently expected. Recent studies have shed some light on how the thermal transport of porous materials could be further reduced by introducing inhomogeneity of the pores. It was reported that inhomogeneous pore sizes or degraded pore distributions led to a significant reduction in the lattice thermal conductivity of porous medium compared to the counterpart with homogeneous porosity [9,10]. The underlying mechanism for this thermal transport deterioration was ascribed to the tortuous conduction path caused by multidimensional pore sizes [11,12]. Studies on the vertically aligned carbon nanotube arrays also revealed that the inhomogeneous distribution of diameter and length could induce increased phonon scattering probability and mismatch, which was another reasonable mechanism for the thermal conductivity reduction [13]. Moreover, since there are huge numbers of interfaces in porous medium, the role of the solid-fluid interfaces or interfaces between adjacent solid particles is a hotspot for investigating the thermal transport for porous materials [14]. From the microscopic viewpoint, the porous ceramic material can be simplified to a three-dimensional lattice of cubic cells and the interfacial thermal conductivity among the crystallites play a dominant role in affecting the overall thermal transport [15]. It was further experimentally confirmed that a higher interfacial thermal conductivity among the connected bronze particles would remarkably boost the thermal conductivity of sintered porous bronze materials [16]. Inspired by the abovementioned up-to-date observations, we could see a great limitation of thermal transport occurring in the materials system with inhomogeneous pore size, and thus we endeavor to reveal the underlying mechanisms for inhomogeneity in influencing the thermal transport and to design the universal porous materials with lower thermal conductivity.

Compared with the vertically aligned carbon nanotube arrays, porous foam materials always render more aspects of inhomogeneity, such as pore size, porosity and pore distribution. Therefore, measuring thermal conductivity accurately and analyzing key factors quantitatively are great challenges, but they continue to spur significant academic interest. Given the complexity and adversity of inhomogeneity involved in porous materials, an attractive strategy combining adaptable interfacial thermos-sensors (AITS) system and 3D tomographic imaging would be applied to study the influence of inhomogeneity in this paper. AITS are devices that can be mated with to closely monitor a material's thermophysical performance, without destroying or limiting the material's integrity, which could enable in situ analyzing heat transfer process [17-19]. Thermal conductivity of typical homogeneous porous materials was extracted by the AITS system, and then microstructure reconstruction was implemented by 3D tomographic imaging. Based on the reconstructed 3D model, an inhomogeneous model is generated by choosing a proper gray value to well represent the sections at the solid-gas interfaces, and the corresponding thermal conductivity could be obtained via the computational simulation. The results obtained in this paper can clearly reveal the quantitative reduction effect of inhomogeneity of pore size distribution on the thermal transport of porous materials, and the proposed approach decouples the stringent practical requirements for further lowering the thermal transport of thermal insulators.

2. Experimental thermal characterization via AITS

2.1 Measurement principle and theory of AITS

As illustrated in Fig. 1a, the self-developed AITS allows reliable and accurate thermophysical measurement of porous thermal insulation materials. By fabricating the sensors on a thermally insulated substrate (PMMA or BK7 glass) with thin silicon nitrides (Si_3N_4) as an interfacial layer, a stable sensor-material contact is formed, while the Printed Circuit Board (PCB) technology is exploited to incorporate the critical signal conditioning and processing functionalities using readily available integrated-circuit components (Fig. 1b). Additionally, high-precision DC Power Source (Aerospace Changfeng Chaoyang Electrical Source Corp. 4NIC-X30 with voltage adjusted rate $\leq 0.5\%$ and ripple voltage amplitude ≤ 10 mV), instrument amplifier (AD620 instead of the conventional Differential Amplifier AMP03) and electric capacitors (10 pF, 1 μF, 100 μF) are mounted to reduce the fluctuation in the readings of the harmonic voltage signals and noise. The Joule heat released from the strip after driven by electric current is the probing signal for thermophysical measurement. Four rectangular pads serve as electrodes for connecting wires outside the sensor. The use of good thermal insulators as the substrate could block the majority of the heat wave signal and thus ensure high sensitivity for probing the thermal insulation materials on the other side of the Au/Cr strip. Since the temperature rise of the strip only relates to the thermal conductivity k and heat capacity C of the substrate and the materials to be measured, it is convenient to calculate the thermal conductivity of the materials from the readings of the transduced voltage signal of the AITS system. The AITS was calibrated with multiple standard specimens with known thermal conductivities at room temperature (Fig. 1c). Results of repeatability and accuracy studies indicate that the measurement error of the thermosensors are within 5.9%, and the measurement range with good accuracy is 0.2~10 W/m K for BK7 glass-based AITS and <0.2 W/m K for PMMA-based AITS. It is clearly found that the AITS presents good accuracy which can rival most commercial measurement methods for thermal conductivity (Table 1).

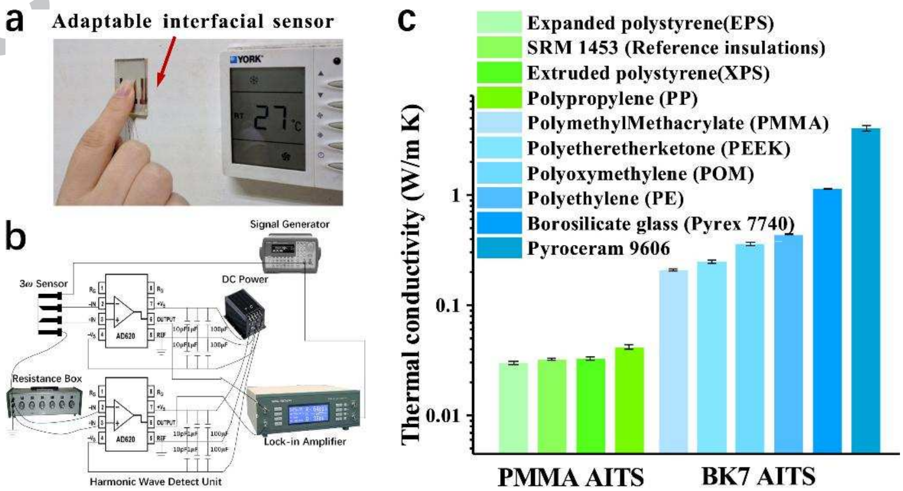

Figure 1 │ Images and schematic illustration of the AITS for k measurement. a, Photograph of a AITS on a material's surface. **b,** Schematic of the total measurement system. The Signal

Generator is an Agilent model 33220A, which also provide a reference signal for the commercial Lock-in Amplifier (Ameteck Signal Recovery 7265). High-precision DC Power Source (Aerospace Changfeng Chaoyang Electrical Source Corp. 4NIC-X30), Instrument Amplifier (AD620), Electric Capacity (10 pF, 1 μF and 100 μF) are mounted in a circuit board. **c,** Thermal conductivity measurement results of various standard materials for the calibration of two types of AITS, indicating small measurement error within 5.9%.

Table 1 Summary of measurement methods, accuracy and standards for the thermal conductivity of typical insulating materials.

Measurement Method	Conductivity (W/m K)	Temperature (℃)	Accuracy	Standards
Guarded Hot Plate	0.01~2	-190 ~ 700	±3%~±5%	GB10294, ASTM C177, ISO 8302
Heat Flow Meter	0.01~10	50 ~ 1400	±5%~±8%	GB10295, ISO 8301 ASTM C518, ASTM E1530
Hot Disk	0.01~500	-269 ~ 200	±5%~±7%	ISO 22007-2:2008
Thermal Capacitance Calorimeter	0.02~2	-180 ~ 1400	±7%~±10%	ASTM E2584
Hot Wire	0.03~30	-196 ~ 1500	±7%~±10%	ASTM C1113, ASTM D5334 ASTM D5930, ISO 8894

The fabrication of AITS utilizes a series of state-of-the-art micro-manufacture techniques, as summarized in Fig. 2. Firstly, the substrate, i.e. PMMA or BK7 glass bulks underwent ultrasonic cleaning in the deionized water for 15 min to get rid of any contaminants. AZ6130 photoresist was spinning coated with a layer of photoresist with 2.4 μm thickness at a speed of 2000 rotation/min. The substrate was baked at 95 ^{o}C for 10 min in order to prompt the evaporation of the solvent within the coated photoresist and thus increased the adhesion between the photoresist and the surface of the substrate. Ultraviolet exposure lasted for 15 seconds and developer solution (tetramethylammonium hydroxide: water = 1:4) was then used for revealing the four-pad micro-sensor pattern. 10 nm thick Cr layer was firstly sputtered under high vacuum (10^{-7} Torr) and Ar atmosphere at flow rate 8 sccm. 200 nm thick Ni layer was then sputtered on the Cr layer under vacuum (2×10^{-3} Torr). Since the conventional acetone would contaminate PMMA surface and even partly dissolve PMMA, dilute alkali solution was deployed to remove the photoresist. Given PMMA can only sustain up to 80 °C, the conventional magnetron sputtering process for deposition of Si_3N_4 protection layer which generally requires 200~300 °C environment could not be used. Thus chemical vapor deposition (CVD) method typically performed at 100 °C was used and the mixture of SiH_4 and NH_3 gases with flow rate 300 sccm and 200 sccm, respectively, were used as the Si_3N_4 source. The deposition process of Si_3N_4 layer stopped every 10 min for cooling (5 min) to ensure non-destruction of the PMMA, and approximately 50 nm thick of Si_3N_4 layer was formed for each operation. After six loops, nearly 300 nm thick Si_3N_4 layer was obtained and the resulted Si_3N_4 layer had uniform thickness distribution and good quality in terms of highly thermally conductive and electrically insulating layer. Silver paste bonding was used to connect the metal wire to the four pads of the micro-sensor.

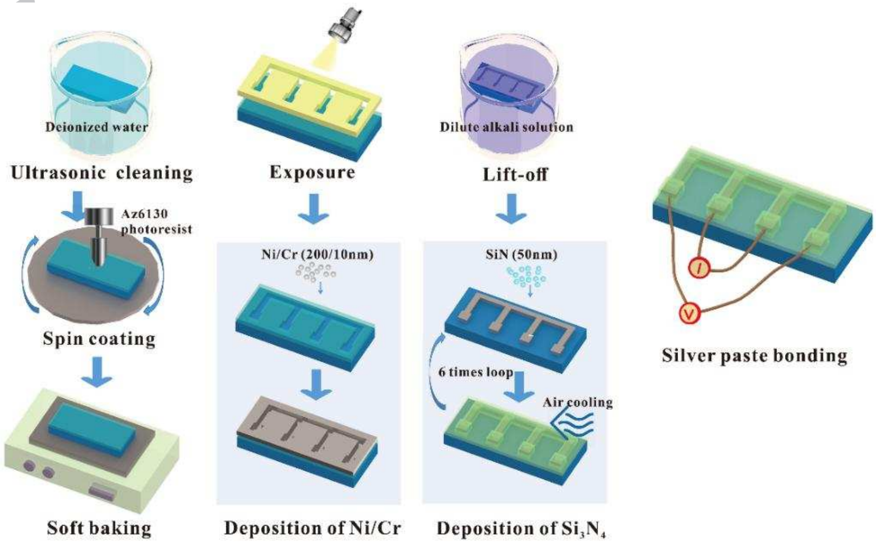

Figure 2 | Process flow for fabrication of AITS for heat transfer characterization.

Nomenclature			
A	area, m	q	complex wave numbers, m^{-1}
b	half width of the 3ω sensor, m	v	volume fraction
C_p	heat capacity, J/m^3 K		
d	sidewall thickness, m	Greek symbols	
F	safety factor	δ	porosity
f	function	η	constant, 0.922
GCI	mesh convergence factor	Φ	gray function
h	size of mesh	Φ_0	gray at the solid-gas interface
i	imaginary number unit	ω	angular frequency, rad/s
k	thermal conductivity, W/m K		
L	length, m	Subscripts	
n	normal vector at the solid-gas interface	eff	effective
p	convergence order of numerical methods	f	gas phase
P	heating power of the sensor, W	g	PMMA plexiglass
Q	heat flow rate, W	s	sample measured, solid phase

The asymmetric nature of the heat diffusion process on two sides of AITS is similar to that proposed by Moon et al. [20] and Gauthier et al. [21]: the electricity-driven metal strip within the 3ω sensor with width 2b and length L releases heat [22] to both sides unequally. However, the above-mentioned precedents only consider the ideal case for which the boundary mismatch is neglected. In contrast, the thermal contact resistance between AITS and porous material (R_c) in our case could become a significant factor that would affect the measured amplitude of the temperature rise. Taking into account the role of R_c, the modified expression for the temperature rise of AITS is:

$$\Delta T = \frac{P/2b}{\sqrt{2\omega C_{pg} k_g} + \dfrac{1}{1/\sqrt{2\omega C_{ps} k_s} + R_C}} e^{-\pi i/4} \quad (1)$$

It is to be noted that at high frequencies, i.e. $\omega \rightarrow \infty$, the above equation could be simplified as $\Delta T = \frac{P/2b}{\sqrt{2\omega C_{pg}k_g} + 1/R_c} e^{-\pi i/4}$, which is consistent with the observed most overlap of experimental data for measurements of the standard sample (amorphous SiO_2 bulk) under different pressure (Fig. 3). At extremely low frequencies, i.e. $\omega \rightarrow 0$, Eq. (1) could be reduced to the following form:

$$\Delta T = \frac{P/2b}{\sqrt{2\omega C_{pg}k_g} + \sqrt{2\omega C_{ps}k_s}} e^{-\pi i/4} \tag{2}$$

The difference in the values of ΔT for different pressure is a direct result of the varied thickness of the test structure. And the effect of the thermal contact resistance between the porous material and the interfacial sensor R_c could be neglected owing to such long thermal penetration depth [23,24] of at frequencies. To cancel out the varied temperature rise at low frequencies under different pressure, we rely on the slope of ΔT versus frequency instead of the absolute values of ΔT to perform the data analysis. By defining F(x) = $-\ln x+\eta$, η=0.922, ΔT is given as:

$$\Delta T = -\frac{P}{\pi(k_s + k_g)} F(q_s b) \times \left[\frac{1}{1 + [k_s/(k_s + k_g)](F(q_s b)/F(q_g b) - 1)} \right] \tag{3}$$

where k_s and k_g represent the thermal conductivity of the sample to be measured and that of the substrate. q is the complex wave numbers or called reciprocal of the thermal penetration depth defied as $q = \sqrt{2\omega C_p i/k}$. According to Eq. (3), thermal conductivity for porous materials with extremely low k is extracted. The thermal conductivity values were extracted by performing least-square fitting algorithm using MATLAB code.

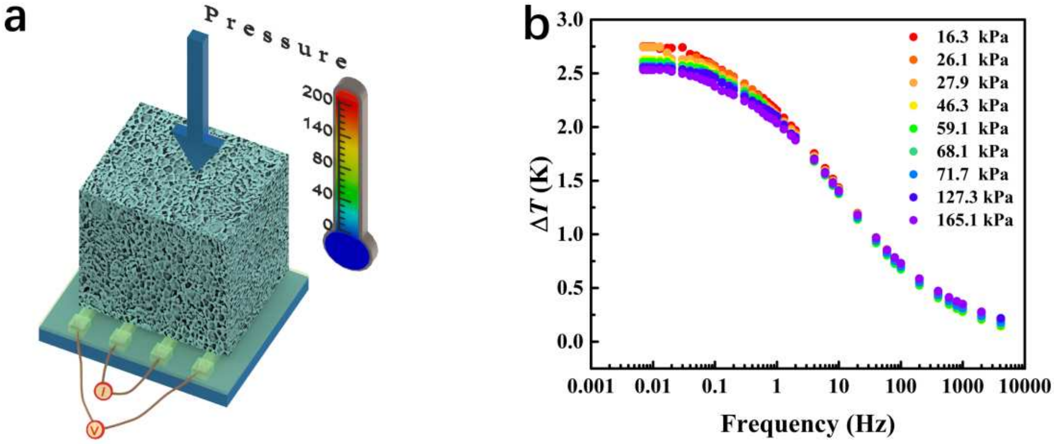

Figure 3 | Test structure of AITS-based 3*ω* method and temperature rise data of AITS for measurement of porous materials. a, Thermal characterization of porous bulks via the AITS-based 3*ω* method under different pressure. **b,** Experimental temperature rise data of AITS under different pressure.

2.2 Characterization of typical porous materials

RS series of polymethacrylimide (PMI) foams was employed for the thermal characterization and modeling. They typically origin from free radical copolymerization of methacrylic acid (MAA) and methacrylonitrile (MAN). Specifically, the copolymerization forms poly (acrylonitrile methyl methacrylate) alternating copolymer (MAA-MAN) sheet, and cyclization and foaming process under heating form the PMI foam. At higher temperature (180~230 ^{o}C), nucleophilic addition reaction occurs between adjacent cyano (CN) and carboxyl (-COOH) in MAA-MAN copolymer, resulting in the formation of the cyclic imide structure with strong polarity and high stiffness, as shown in Fig. 4a. The thermal conductivity of a series of RS foams with various densities, i.e. 30.0 kg/m^3, 45.0 kg/m^3, 100 kg/m^3, 120 kg/m^3 and 200 kg/m^3 (corresponding porosity δ are 97.0%, 95.5%, 90.0%, 88.0% and

80.0% calculated by comparing the density of foams with that of the pure solid element of around 1000 kg/m^3) were measured via PMMA-based AITS, and was found to show increasing slope of the third voltage vs. frequency trend with the increased porosity (Fig. 4b). Figure 4c demonstrates the microscopic morphology structure of RS series from scanning electron microscope (SEM), indicating the closed rates are larger than 99% and the average pore size are statistically around 200 μm.

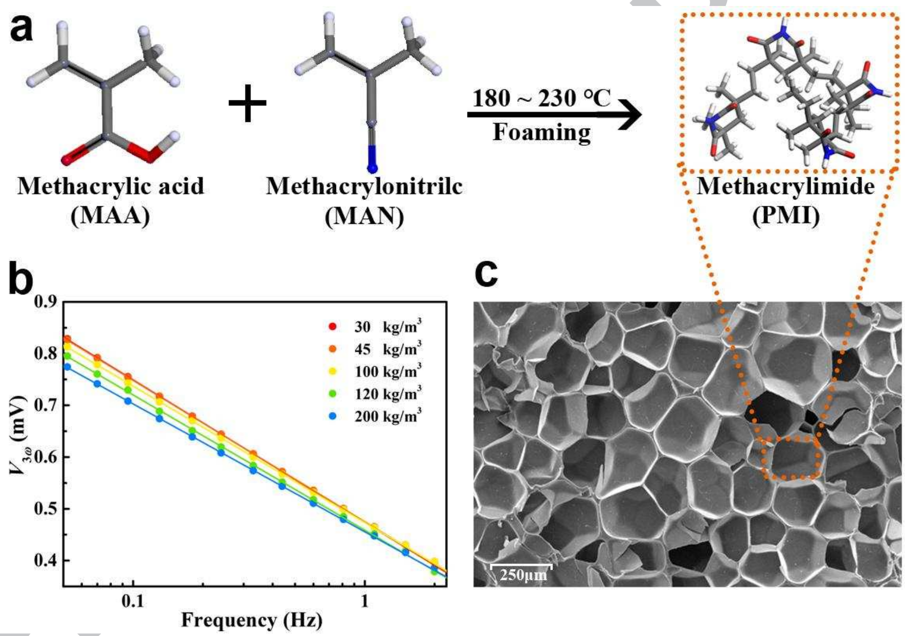

Figure 4 │ Synthesis process and experimental data of thermal characterization for representative porous material. a, Synthesis process of RS series of PMI foams. **b,** experimental measurement data of RS foams with different densities via the AITS-based 3ω method. **c,** representative SEM image for RS series of PMI foams.

3. Heat transfer modeling

3.1 Conventional heat transfer models

The models for describing the heat transfer process of porous materials have developed into multiple choices. The most conventional candidates are two-dimensional (2D) series model, parallel model, Effective Medium Theoretical (EMT) model, Bruggeman model, and Maxwell-Eucken (ME) model [7,25-27]. Parallel and series models are the simplest and ideal cases, which represent the upper and lower limits, respectively. In fact, the thermal conductivity of porous materials falls between these two models. Maxwell model was firstly verified for Maxwell spherical particle composites by analogy with the electrical conductivity equation [25]. And it assumes that the spherical particles with identical diameters are dispersed without rules in a matrix and no interaction exists between each other. Maxwell model is believed to be a universal model which is not only applicable for dispersed particles within matrix but also for porous insulations. In contrast, Bruggeman model [26] is applicable for composite materials containing particles with high concentration. It assumes the interaction between particles could be solved by gradually increasing the number of dispersed particles, and thus is typically used for materials with high particle fraction. Another widely used model, i.e. EMT model [27], assumes random distribution of various phases within the specific composite material, and thus exhibits strong inhomogeneity in the pore size distribution. In that case, each components would randomly connect or disconnect with the others. Table 2 summarized the schematics and mathematical expressions for the above-mentioned models.

Table 2 Mathematical expressions for various models to describe the heat transfer of thermal insulation materials

Model	Schematics	Mathematical expressions	Model	Schematics	Mathematical expressions

Series	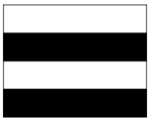	$k_{eff} = \frac{k_s k_f}{\delta k_s + (1-\delta) k_f}$ [7]	Parallel	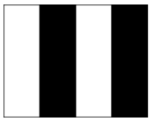	$k_{eff} = (1-\delta) k_s + \delta k_f$ [7]
Maxwell-Eucken (ME)	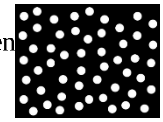	$k_{eff} = k_s \frac{2k_s + k_f - 2(k_s - k_f)\delta}{k_s + k_f + (k_s - k_f)\delta}$ [25]	Bruggeman	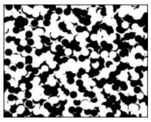	$k_{eff} = k_f + \frac{k_f (1-\delta)^3 (k_s - k_f)}{k_s}$ [26]
EMT	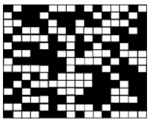	$k_{eff} = 1/4\left(A + \sqrt{A^2 + 8k_s k_f}\right)$, $A = (3\delta - 1)k_f + [3(1-\delta) - 1]k_s$ [27]	Hollow Cube	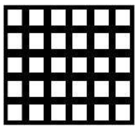	$k_{eff} = \frac{L}{L-2d}\delta k_f + \frac{4d(L-d)}{L^2} k_s$ [28]

Note: k_s represents the thermal conductivity of the matrix material, k_f represents the thermal conductivity of spherical filling material, δ is the volumetric ratio of the filling material.

3.2 Simulation based on homogeneous model

Hollow cube model [28], which is frequently employed to describe the thermal transport of porous materials, has embraced a success for accurate simulation of the heat transfer process of homogeneous aluminum foams [29]. The typical unit cell of hollow cube model is regarded as a combination of cube wall (sidewall of the foams) and inner smaller cube (the filled gas). The edge length of the cube, L, is estimated statistically by using average size of the unit, approximately 200 μm. The wall thickness is obtained based on the porosity δ data obtained experimental and the equation $\delta = (L-2d)^3 / L^3$. According to the structure parameters for the hollow cube model, mesh models are generated for RS foams with different porosities via the Gambit® software. To ensure the accuracy of simulation, the mesh at the wall-gas interfaces was intensified and then imported to Fluent® software. Taking into account the fact that RS foams originates from chemical reaction of different components and foam molding, the thermal conductivity of solid matrix is using a value of 0.25 W/m K via comparing the experimental data and Maxwell model. By setting the following boundary conditions: (i) the temperature are constant at z=0 and z=200 μm locations; (i) the other outer interfaces are insulated; (iii) the solid-gas interfaces are subject to convection and conduction coupled conditions, the heat flow rate Q through the cross-section could be obtained according to the simulation. Therefore, the effective thermal conductivity of RS foams is calculated according to the Fourier Law of Heat Conduction: $k_{eff} = \frac{QL}{A(T_1 - T_2)}$, $(T_1 > T_2)$. Figure 5a,b schematically shows the unit of hollow cube model and Fig. 5c presents calculation results from Fluent® software, i.e. the steady temperature distribution of the model under the temperature difference of 10 °C, which was then used to extract thermal conductivity k_{eff} for the specimen. Figure 5d shows the k versus porosity trend for RS foams.

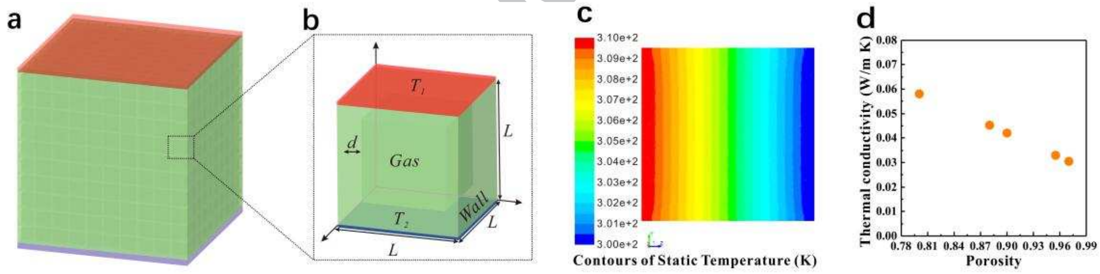

Figure 5｜**Hollow cube model for heat transfer analysis. a,** Schematic for hollow cube model. **b,** the enlarged view for the unit cell **c,** the simulated temperature distribution under steady heat conduction. **d,** calculated thermal conductivity versus porosity.

3.3 Simulation method for constructing inhomogeneous model

X-ray tomographic imaging technique was utilized as a powerful approach for the construction of inhomogeneous microstructure model for the RS foams investigated [30-32]. Typically, a sequence of fracture images was used to form the morphological data for the reconstruction of the three dimensional (3D) matrix of the material based on the micro-CT scanning technique. Software Simpleware® was used to process the data and export the gray function Φ(x, y, z) of the whole scanned region. A proper gray value Φ_0 was chosen to represent the solid-gas interface and used to obtain the inhomogeneous 3D structure of the porous specimen. The scanned regions of the specimen were larger than ten times of the pore sizes to ensure the convergence of the thermal conductivity to be calculated. Given the average pore size of the investigated RS foam is around 200 μm, cubic space with side-length of approximately 4 mm are scanned. The steady heat conduction equation for the solid and gas phases are:

$$\nabla \cdot [k_s \nabla T_s] = 0 \tag{4}$$

$$\nabla \cdot [k_f \nabla T_f] = 0 \tag{5}$$

The boundary conditions are:

$$T_s = T_f \tag{6}$$

$$n \cdot k_s \nabla T_s = n \cdot k_f \nabla T_f \tag{7}$$

where T_s and T_f are the temperatures of solid and gas, respectively. k_s and k_f are the thermal conductivity of solid and gas, n is the normal vector at the solid-gas interface.

The studied object is divided by using orthogonal grid, and discrete finite element method is employed for solving the above control equation. The expression of the effective thermal conductivity is:

$$k_{eff} = \frac{\int_0^{A_s} k_s \nabla T_s \cdot n dA_s - \int_0^{A_f} k_f \nabla T_f \cdot n dA_f}{(T_1 - T_2)(A_s + A_f)} \tag{8}$$

To ensure that the result is independent of the mesh, relatively sparse grid is used at the initial stage and denser grid is gradually deployed which would finally get converged temperature fields. The criteria of convergence is:

$$GCI = F\left|\frac{k_{eff,h} - k_{eff,2h}}{k_{eff,h}}\right| \Big/ \left(2^p - 1\right) \tag{9}$$

where GCI is mesh convergence factor, subscript h and 2h represent the size of mesh, F is safety factor, p is the convergence order of numerical methods. We used F=1.25 and p=2 in this study. When GCI<5%, the divided mesh could be applied to simulate the heat transfer process.

It is to be noted that this technique is difficult to discern the solid and gas phases for the specimens with extremely small pores, such as the case for RS foams with such high porosity as 97.0%. However, for lower porosity and correspondingly large pore size, typically for porosity lower than 95.5%, the morphology of RS foam can be excellently reconstructed (Fig. 6a). One merit of this technique is the distribution of thermal conductivity along 3D directions could be readily calculated based on finite element method. We have considered the difference in uniformity of three dimensional distribution of pores in the inhomogeneous model. After we rebuilt the inhomogeneous 3D porous structures, there was indeed non-uniformity of three dimensional distribution of the pores which was confirmed via the discrete finite element method. The calculated thermal conductivity k for three dimensions indicated a slight difference for four RS foams and the maximum relative deviation for k was 5.88% (Table 3). The final result we presented is the average value of all directions since the microscopic structure along x, y and z direction are close to each other, reflected by the error bar in Fig. 6b.

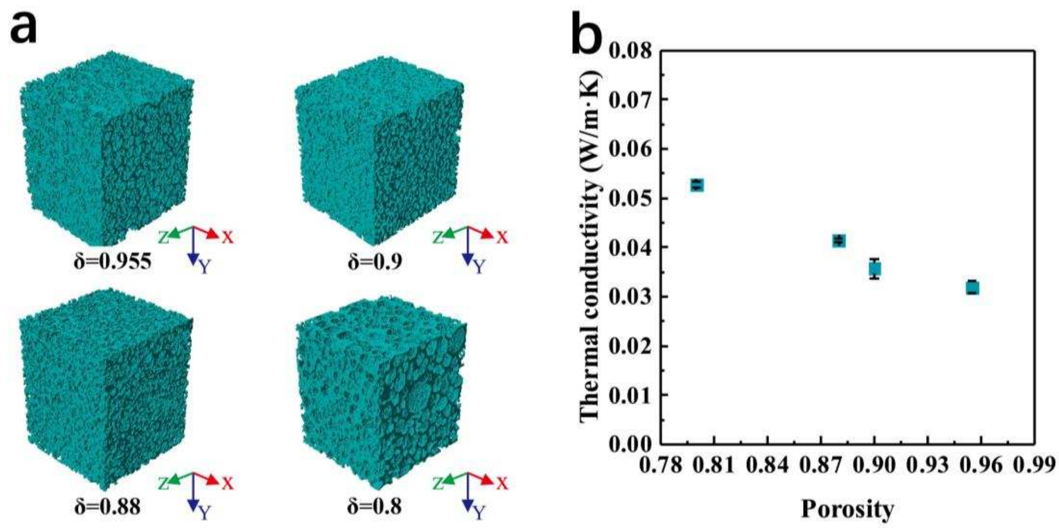

Figure 6 | CT scanning imaging for building inhomogeneous microstructure to perform heat transfer analysis for RS foams with varied porosities. a, reconstructed images for further data processing. **b,** the averaged thermal conductivity based on our 3D simulation. The error bar is calculated using the thermal conductivity values of x, y and z directions.

Table 3 The calculated direction-dependent thermal conductivity based on three dimensional inhomogeneous distribution of pores

ρ kg/m^3	δ %	k_x W/(m·K)	k_y W/(m·K)	k_z W/(m·K)	k_{ave} W/(m·K)	Maximum Deviation %
200	80.0	0.0527	0.0523	0.0533	0.0527	0.945
120	88.0	0.0416	0.0415	0.0410	0.0414	0.966
100	90.0	0.0378	0.0339	0.0355	0.0357	5.88
45.0	95.5	0.0333	0.0309	0.0315	0.0319	4.39

4. Results and Discussion

Figure 7 demonstrated the evolution trend of the measured thermal conductivity versus porosity for RS foams and the predicted curves from various heat transfer models. It is clearly shown that the parallel model and series model are still representing the Upper Limit (UL) and Lower Limit (LL) for the thermal conductivity trend as usual. The predicted k versus δ curve for RS foams from EMT model agrees well with the experimental data for samples with very high porosity, but it is remarkably lower than that with relatively lower porosities. The underlying reason is EMT model deploys tiny squares to construct the matrix (Table 2), which brings about huge inhomogeneity of pore size and pore distribution, and thus renders lower prediction similar to series model.

The inhomogeneous model which originates from CT scanning reconstruction technique also appreciably underestimated k values, owing to the gray value Φ_0 representing the solid-gas interface. It is to be noted that the chosen gray value could neglect some tiny connections of solid skeleton and thus generate non-homogeneous pores during the reconstruction process, a main culprit for undermining the thermal transport. The inhomogeneous model from CT scanning reconstruction agree well with that from the 2D Bruggeman model, further validate the reconstructed 3D morphology of RS foams based on CT scanning technique merged with special processing of the solid-gas interface, would unavoidably loss some tiny solid-solid interfacial connection structures and thus generate inhomogeneous pores. In marked contrast, the typical homogeneous model, i.e. 2D Maxwell model and 3D hollow cube model, suggest a perfect agreement with the measured k versus δ evolution trend. The appreciable reduction up to 13.5% for the thermal conductivity could be realized due to the inhomogeneity in pore size distribution. However, the increase in the porosity would undermine the role of the inhomogeneity as shown in Fig. 7. It has been experimentally verified that increasing the porosity (or decreasing the density) and doping heterogeneous atoms could attain a similar reduction in the thermal conductivity for some typical porous material. For example, a reduction of 10.8% in k for aqueous etched porous silicon wafer was reported by increasing the porosity from 43% to 66% using the solution containing 4.8% HF and 0.1 wt.% ionic surfactant [33]. Similarly, a reduction of 18.3% in k was found for porous carbon aerogels via lowing its density from 0.128 g/cm^3 to 0.066 g/cm^3 [34]. Boron doping could also induce an approximately 14.8% reduction of k for porous film [35]. According to these previous reports, we could conclude that constructing inhomogeneous distribution of pores would achieve the similar effect compared with increasing porosity and doping heterogeneous atoms.

In addition, it is intuitive to draw the conclusion that the real morphology of RS foam based on SEM imaging (Fig. 4c) is a rigorously closed structure consisting of periodic polyhedral cells. Although the polyhedral cell includes multiple shapes, such as quadrilaterals, pentagons, hexagons and heptagons, the simplification treatment of the shapes to be identical circular (2D Maxwell model) and square (3D hollow cube model) would not induce discernable deviation for modeling the thermal transport (Fig. 7). Therefore, for the case that it is difficult to obtain higher porosity for the porous materials, developing inhomogeneity in pore size distribution during the fabrication process of the materials would be a promising approach for realization of lower thermal transport to meet the stringent requirement of super thermal insulations.

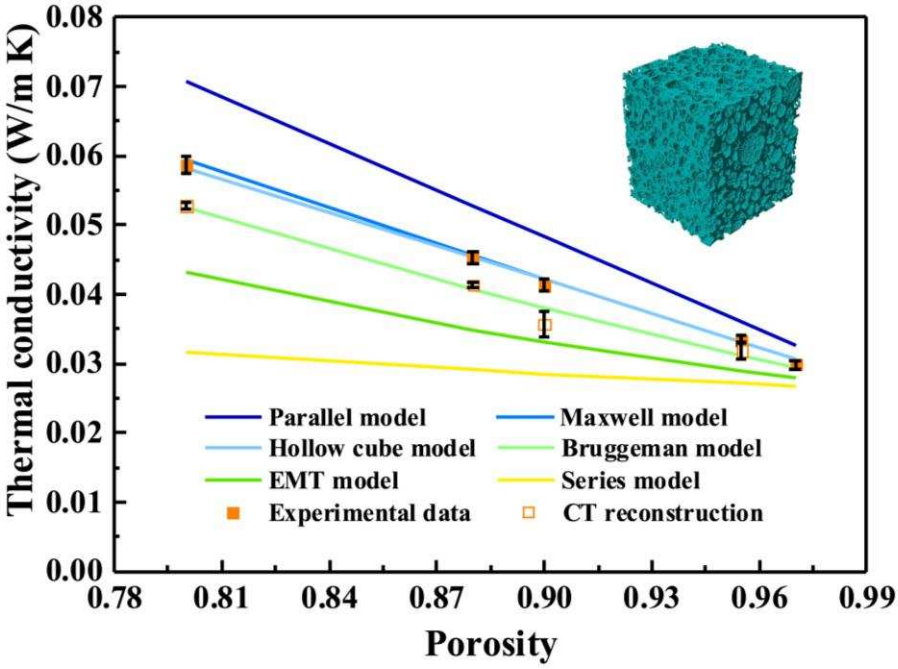

Figure 7 | Comparison of experimental and calculated porosity dependence of thermal conductivity based on homogeneous and inhomogeneous heat transfer models for RS foams.

5. Conclusion

In this paper, we have evaluated the effect of inhomogeneous pore distribution on the thermal transport of porous materials at a quantitative level. By developing fully adaptable interfacial thermos-sensor merged with commercially available integrated circuit components, the apparent thermal conductivity versus porosity relation of RS foams consisting of periodic polyhedral cells was accurately measured. The comparison of thermal conductivities between homogeneous and inhomogeneous porous materials was attained through 3D tomographic modeling to generate inhomogeneous microstructure and finite element method to calculate the thermal conductivity. 2D and 3D reconstruction modeling for heat transfer analysis of the RS foams indicate that the inhomogeneity of pore size distribution would cause an additional reduction up to 13.5% of thermal transport for typical porous materials. Importantly, the distinction between the homogeneous and inhomogeneous models would remarkably diminish as the porosity approaches to a very high value, probably owing to the increment of the volume of the solid-gas interface. We envision that the quantitative result of the reduction by inhomogeneity of pore size could shed a light on developing of super thermal insulation materials.

Acknowledgements

This research is supported by National Natural Science Foundation of China (No. 51306183 and 51422601) and the Fundamental Research Funds for the Central Universities. Lin Qiu and Dongsheng Wen are grateful for the support from the Royal Society via its International Exchanges program.

References

[1] Yang L, Yang N, Li B. Extreme low thermal conductivity in nanoscale 3D Si phononic crystal with spherical pores. Nano Lett 2014;14(4):1734-8.

[2] He Y, Donadio D, Galli G. Morphology and temperature dependence of the thermal conductivity of nanoporous SiGe. Nano Lett 2011;11(9):3608-11.

[3] Cui B, Zeng L, Keane D, Bedzyk MJ, Buchholz DB, Chang RPH, Yu X, Smith J, Marks TJ, Xia Y, Facchetti AF, Mededeva JE, Grayson M. Thermal conductivity comparison of indium gallium zinc oxide thin films: Dependence on temperature, crystallinity, and porosity. J Phys Chem C 2016;120(14):7467-75.

[4] Qiu L, Li YM, Zheng XH, Zhu J, Tang DW, Wu JQ, Xu CH. Thermal-conductivity studies of macro-porous polymer-derived SiOC ceramics. Int J Thermophys 2014;35(1):76-89.

[5] Shimizu T, Matsuura K, Furue H, Matsuzak K. Thermal conductivity of high porosity alumina refractory bricks made by a slurry gelation and foaming method. J Eur Ceram Soc 2013;33(15):3429-35.

[6] Perez-Taborda JA, Rojo MM, Maiz J, Neophytou N, Martin-Gonzalez M. Ultra-low thermal conductivities in large-area Si-Ge nanomeshes for thermoelectric applications. Sci Rep 2016;6:32778.

[7] Qiu L, Zheng XH, Zhu J, Tang DW, Yang SY, Hu AJ, Wang LL, Li SS. Thermal transport in high-strength polymethacrylimide (PMI) foam insulations. Int J Thermophys 2015;36(10):2523-34.

[8] Wicklein B, Kocjan A, Salazar-Alvarez G, Carosio F, Camino G, Antonietti M, Bergström L. Thermal insulating and fire-retardant lightweight anisotropic foams based on nanocellulose and graphene oxide. Nature Nanotech 2015;10(3):277-83.

[9] Tarkhanyan RH, Niarchos DG. Reduction in lattice thermal conductivity of porous materials due to inhomogeneous porosity. Int J Therm Sci 2013;67(5):107-12.

[10] Tarkhanyan RH, Niarchos DG. Reduction of thermal conductivity in porous “gray” materials. APL Mater 2014;2(7):076107.

[11] Alam MK, Druma AM, Druma C. Thermal transport in graphitic carbon foams. J Compos Mater 2004;38(22):1993-2006.

[12] Harfash AJ. Three-dimensional simulations for convection problem in anisotropic porous media with nonhomogeneous porosity, thermal diffusivity, and variable gravity effects.

Transport Porous Med 2014;102(1):43-57.

[13] Bauer ML, Pham QN, Saltonstall CB, Norris PM. Thermal conductivity of vertically aligned carbon nanotube arrays: Growth conditions and tube inhomogeneity. Appl Phys Lett 2014;105(15):151909.

[14] Wang M, Wang J, Pan N, Chen S. Mesoscopic predictions of the effective thermal conductivity for microscale random porous media. Phys Rev E 2007;75(3):036702.

[15] Smith DS, Alzina A, Bourret J, Nait-Ali B, Pennec F, Tessier-Doyen N. Thermal conductivity of porous materials. J Mater Res 2013;28(17):2260-72.

[16] Miettinen L, Kekäläinen P, Turpeinen T, Hyväluoma J, Merikoski J, Timonen J. Dependence of thermal conductivity on structural parameters in porous samples. AIP Adv 2012;2(1): 012101.

[17] Gao W, Emaminejad S, Nyein HY, Challa S, Chen K, Peck A, Fahad HM, Ota H, Shiraki H, Kiriya D, Lien DH, Brooks GA, Davis RW, Javey A. Fully integrated wearable sensor arrays for multiplexed in situ perspiration analysis. Nature 2016;529(7587):509-14.

[18] Dittmar A, Pauchard T, Delhomme G, Vernet-Maury E. A thermal conductivity sensor for the measurement of skin blood flow. Sensors Actuat B-Chem 1992;7(1-3):164-73.

[19] Wu X, Ma Y, Zhang G, Chu Y, Du J, Zhang Y, Li Z, Duan Y, Fan Z, Huang Jia. Thermal stable, biocompatible, and flexible organic field-effect transistors and their application in temperature sensing arrays for artificial skin. Adv Funct Mater 2015;25(14):2138-46.

[20] Moon IK, Jeong YH, Kwun SI. The 3ω technique for measuring dynamic specific heat and thermal conductivity of a liquid or solid. Rev Sci Instrum 1996;67(1):29-35.

[21] Gauthier S, Giani A, Combette P. Gas thermal conductivity measurement using the

three-omega method. Sensor Actuat A-Phys 2013;195:50-5.

[22] Qiu L, Tang DW, Zheng XH, Su GP. The freestanding sensor-based 3ω technique for measuring thermal conductivity of solids: principle and examination. Rev Sci Instrum 2011;82(4):045106.

[23] Koh YK, Singer SL, Kim W, Zide JMO, Lu H, Cahill DG, Majumdar A, Gossard AC. Comparison of the 3ω method and time-domain thermoreflectance for measurements of the cross-plane thermal conductivity of epitaxial semiconductors. J Appl Phys 2009;105(5):054303.

[24] Mishra V, Hardin CL, Garay JE, Dames C. A 3 omega method to measure an arbitrary anisotropic thermal conductivity tensor. Rev Sci Instrum 2015;86(5): 054902.

[25] Maxwell JC. A Treatise on Electricity and Magnetism. Dover, New York; 1954.

[26] Tso CY, Fu SC, Chao CYH. A semi-analytical model for the thermal conductivity of nanofluids and determination of the nanolayer thickness. Int J Heat Mass Transfer 2014;70:202-14.

[27] Landauer R. The electrical resistance of binary metallic mixtures. J Appl Phys 1952;23(7):779-84.

[28] Coquard R, Baillis D. Numerical investigation of conductive heat transfer in high-porosity foams. Acta Mater 2009;57(18):5466-79.

[29] Ma MY, Ye H. An image analysis method to obtain the effective thermal conductivity of metallic foams via a redefined concept of shape factor. Appl Therm Eng 2014;73(1):1279-84.

[30] Fiedler T, Solórzano E, Garcia - Moreno F, Öchsner A, Belova IV, Murch GE. Computed tomography based finite element analysis of the thermal properties of cellular aluminium. Materialwiss Werkst 2009;40(3):139-43.

[31] Veyhl C, Belova IV, Murch GE, Öchsner A, Fiedler T. Thermal analysis of aluminum foam based on micro-computed tomography. Materialwiss Werkst 2011;42(5):350-5.

[32] Mendes MAA, Ray S, Trimis D. A simple and efficient method for the evaluation of effective thermal conductivity of open-cell foam-like structures. Int J Heat Mass Transfer 2013;66:412-22.

[33] Boor JD, Kim DS, Ao X, Hagen D, Cojocaru A, Föll H, Schmidt V. Temperature and structure size dependence of the thermal conductivity of porous silicon. EPL-Europhys Lett 2011;96(1):16001.

[34] Feng J, Feng J, Zhang C. Thermal conductivity of low density carbon aerogels. J Porous Mater 2012;19(5):551-56.

[35] Tang J, Wang HT, Lee DH, Fardy M, Huo Z, Russell TP, Yang P. Holey silicon as an efficient thermoelectric material. Nano Lett 2010;10(10):4279-83.

Highlights

- Quantitative degradation effect of inhomogeneity in pore size is first revealed.
- Adaptable interfacial sensor technology is proposed to ensure accurate measurement.
- Ample models of heat transfer are compared to extract the inhomogeneity effect.
- This study opens up fresh opportunities for developing super thermal insulators.